Essay
MAP-Fis 2024-2025

A Quest for Physical Observables in Quasiperiodic Moiré Systems

Raul Liquito

Supervisors:
Prof. Eduardo V. Castro
Miguel Gonçalves

Departamento de Física e Astronomia,

Faculdade de Ciências da Universidade do Porto

Porto, Abril 2025

Abstract

In recent years, the study of moiré materials has been established as one of the richest fields of condensed matter physics. A prime example of a moiré material is Twisted Bilayer Graphene (tBLG), which exhibits exotic physical properties, such as unconventional superconductivity and other intriguing strongly-correlated phases. For most twist angles, tBLG is quasiperiodic, lacking translational invariance, a feature typically overlooked by the scientific community. More recently, moiré of moiré systems have also gathered attention. An example is Twisted Trilayer Graphene (tTLG), quasi-periodic for most twist angles. The super-moiré poses a competition between different moiré scales, enhancing the quasiperiodic effects. Naturally, a central question emerges: what is the role of quasi-periodicity on moiré materials, and how can experimentalists distinguish quasiperiodic and commensurate[1] structures? The goal of this project is to simulate moiré materials accounting for the important but often ignored quasiperiodicity, focusing on experimentally accessible observables capable of capturing the rich electronic properties of quasiperiodic systems.

---

[1] Periodic

Contents

1 Introduction **4**

1.1 The Era of Graphene 4

1.2 The birth of Moiré Materials 5

2 State of Art **8**

2.1 Moiré systems 8

2.2 Atomic Quasiperiodicity in Moiré systems 8

2.3 Lattice Relaxation in Moiré materials 10

2.4 Transport 11

2.5 Experimental measurements 12

3 Research proposal **15**

3.1 Main Goals 15

3.2 Challenges and Methodology 16

3.3 Work Plan 17

Bibliography **18**

Chapter 1

Introduction

1.1 The Era of Graphene

Graphene is a sheet of carbon atoms arranged on a honeycomb structure. Each atom contributes one s-orbital and two p-orbitals that hybridize to form three sp^2 orbitals. These form strong σ-bonds with neighboring atoms spaced $1.42\AA$ apart. These bonds are responsible for the material's mechanical strength and structure stability leading to the formation of σ-bands. The remaining unhybridized p-orbitals overlap with those of adjacent atoms to form π-bonds, resulting in the half-filled π-band. The π-bonding is responsible for graphene's remarkable electronic properties, including its linear low-energy dispersion and high carrier mobility.

In 1947, P. R. Wallace performed the first theoretical study of graphene's band structure, accurately predicting its semi-metallic behavior [1]. Despite the significance of Wallace's work, the scientific community remained skeptical regarding the viability of two-dimensional materials due to the disseminated belief that atomically thin structures were thermodynamically unstable and prone to collapse as argued by Peierls and Landau [2, 3]. Nonetheless, theoretical studies of carbon allotropes gained popularity after Wallace's publication, and attention shifted to graphite – a three-dimensional material composed of stacked graphene layers coupled via weak Van der Waals forces, allowing it to retain some of the electronic properties of graphene.

In 2004, a breakthrough occurred when Novoselov and collaborators [4] successfully isolated and measured the electronic properties of graphene (see Fig. 1.1). The samples were obtained through mechanical exfoliation of highly oriented pyrolytic graphite and deposited on silicon wafers of silicon dioxide (SO_2), a semiconductor. The silicon wafer played two distinct roles. First, the graphene sheets could be visible with optical microscopes when the wafer had the proper thickness (roughly $300nm$). Secondly, silicon dioxide was a key substrate that electrically isolated the graphene sample while coupling weakly to graphene, thereby preserving its intrinsic electronic properties and enabling accurate transport measurements. Novoselov and Geim's achievements earned them the 2010 Nobel Prize in Physics and paved the way for the Era of Graphene.

The wonder material, as it became known, exhibits a wide range of exotic electronic properties, the most notable being the presence of linearly dispersing electrons known as Dirac fermions (see Fig 1.2). These are described by a Dirac-like equation, exhibiting physics analogous to quantum electrodynamics (QED), albeit with a Fermi velocity of $v_f \approx 10^6 m/s$, which is significantly

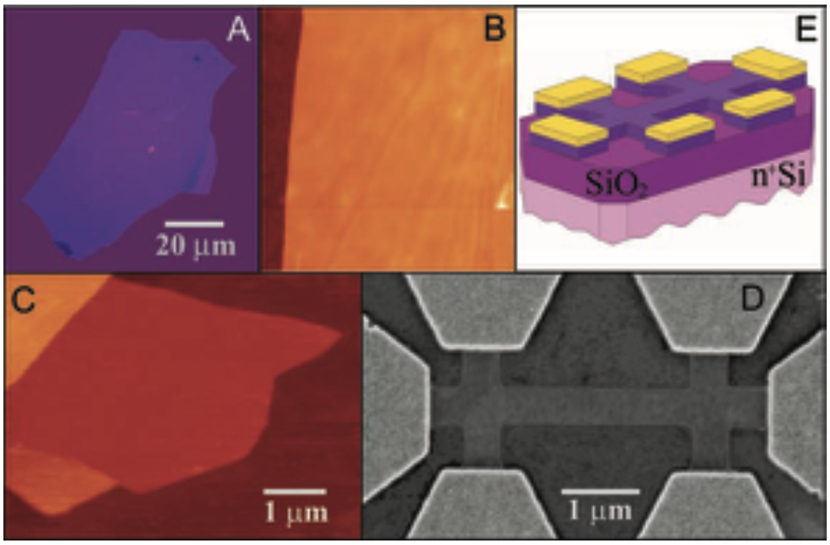

Figure 1.1: Graphene films. **(A)** Photograph (in normal white light) of a relatively large multilayer graphene flake on top of an oxidized Si wafer. **(B)** Atomic force microscope(AFM) image of $2 \mu m$ by $2 \mu m$ area of this flake near its edge. Colors: dark brown,SiO_2 surface; orange, $3nm$ height above the SiO2 surface. **(C)** AFM image of single-layer graphene. Colors: dark brown, SiO_2 surface; brown-red (central area), $0.8nm$ height; yellow-brown (bottom left), $1.2nm$; orange (top left), $2.5nm$. **(D)** Scanning electron microscope image of one of experimental devices prepared from FLG. **(E)** Schematic view of the device in (D). This image and the description were adapted from [4].

smaller than the speed of light. The Dirac-like nature of graphene's electrons is responsible for its exotic electronic properties, including room temperature integer quantum Hall effect (IQHE) [5], robustness to electrostatic potentials [6, 7], immunity to electron localization [8], and micrometer scale scattering length [4]. At the mesoscopic scale, the Dirac fermions also enable ballistic transport and support supercurrent flow when graphene is contacted by superconducting leads [9].

1.2 The birth of Moiré Materials

Novoselov's 2004 work [4] marked the beginning of the modern field of two-dimensional materials. Not only did he demonstrated that atomically thin crystals could exist as stable structures, but the experimental results matched long-standing theoretical predictions. This ignited research in 2D materials generating novel experimental techniques. One fundamental method is electrostatic voltage gating, which allows precise control over carrier density without altering the material chemical composition (chemical doping). Since then these materials have been a great focus of research in condensed matter physics, stemming from their exotic electronic properties and the easily accessible bulk – unlike in conventional three-dimensional systems – making them ideal platforms for fundamental studies and device applications.

The scientific community's focus shifted towards stacking atomically thin layers, known as multilayer materials, enabling access to a wide range of previously unexplored phases of matter. Early efforts concentrated on AA and AB stacked graphene, which were the easiest to produce. In 2007, João Lopes dos Santos *et. al.* [11] introduced a theoretical model for two graphene layers stacked with a small relative twist angle, thus laying the foundation for twisted bilayer graphene

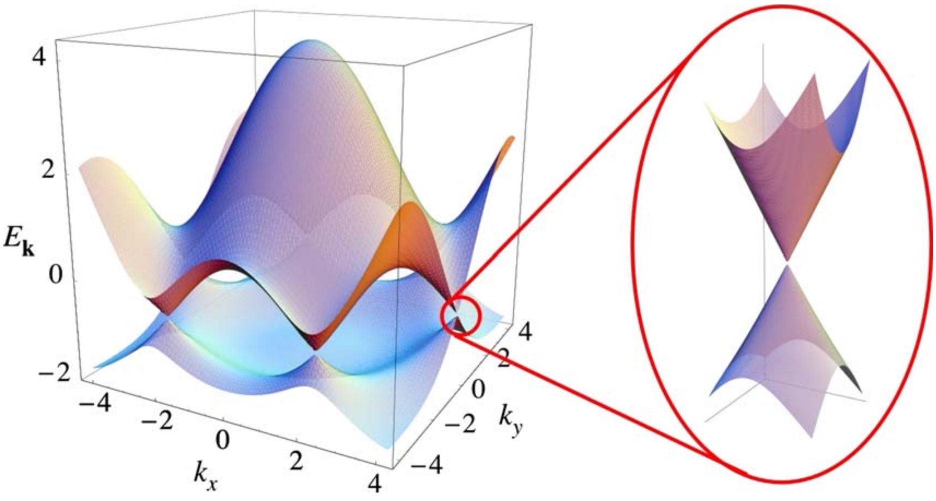

Figure 1.2: Electronic dispersion in the honeycomb lattice. **Left**: Energy spectrum in units of hopping amplitude (t) , with $t = 2.7eV$. **Right**: Zoom in of the energy bands close to one of the Dirac points. This image was adapted from Ref. [10].

(tBLG). The relative twist misaligns the two layers, producing an interference pattern known as a moiré pattern, previously observed in the 1980's through scanning tunneling microscopy measurements of graphite [12]. The first experimental observation of tBLG was in 2010 [13] via scanning tunneling microscopy and spectroscopy (STM and STS) measurements, where the key finding was the ability to tune the Van Hove singularities (VHS) to be arbitrarily close to the Fermi level.

In two-dimensional materials, VHS appear from saddle points in the band structure. However, in graphene, they occur at energies outside the range of current gating or doping methods[10]. Near a VHS the Fermi velocity is suppressed, thus electron-electron interactions are expected to dominate. The ability to bring the VHS arbitrarily close to the Fermi level – by adjusting the twist angle – was a significant milestone in moiré physics. Notably, in tBLG, the VHS merge and a flatband appears, leading to the suppression of the Fermi velocity at a particular set of twist angles known as the magic angles, with the largest being $\theta \approx 1.1^{\underline{\text{o}}}$ [11, 14, 15] . Although the work presented in Ref. [13] did not prove the existence of magic angles due to the lack of twist angle control in chemical vapor deposition (CVD), it hinted at the possibility of merging the VHS into one flatband.

In 2011, Rafi Bistritzer and Allan H. MacDonald [15] developed a continuum model for tBLG, which indicated the existence of magic angles. Their work led to the prediction of correlated phases in magic angle tBLG [16, 17]. Despite these predictions, experimentalists had no method capable of freely tuning the twist angle between layers and were stuck with techniques like CVD that produced samples with random twist angles. This paradigm changed with the development of the "tear-and-stack" technique [18] that allowed precise alignment of multilayer systems. This advancement was crucial for the work of Pablo Jarillo-Herrero's group, which demonstrated the appearance of unconventional superconductivity in magic-angle twisted bilayer graphene (MAtBLG) at very low temperature ($\approx 100mK$)[19].

The key discoveries of the last two decades set the stage for one of the most exciting eras in condensed matter physics.

Chapter 2

State of Art

2.1 Moiré systems

Moiré systems are two-dimensional materials formed by stacking atomically thin crystals with a relative twist angle or different lattice parameters. These misalignments generate an interference pattern, the moiré pattern, which drastically reshapes the electronic band structure of the material. In twistronics, the twist angle serves as a tuning knob allowing control of the electronic properties of moiré crystals. To date, a wide variety of multilayer structures have been experimentally realized and studied, including twisted bilayer graphene [13, 19–22], twisted trilayer graphene (tTLG) [23–27], twisted bilayer borophene (tBLB) [28], and twisted transition metals dichalcogenides (TMD) [29–37].

Twisted bilayer graphene is the prototypical moiré material, consisting of two stacked graphene layers with a relative twist angle. This twist generates a Moiré interference pattern with a characteristic length scale that can reach hundreds of nanometers. The electronic properties of tBLG are sensitive to changes in twist angle. For large twist angles ($\theta > 10^{\text{o}}$), interlayer tunneling is suppressed, leading to electronic properties similar to that of individual graphene [15, 38], with the exception of the quasicrystal tBLG observed at $\theta = 30^{\text{o}}$. In contrast, at small twist angles, the interlayer tunneling renormalizes the band structure of graphene. In particular, at the largest magic angle $\theta \approx 1.16^{\text{o}}$, the Fermi velocity goes to zero, the gap to the dispersive remote bands is at its maximum and a nearly flat band appears [11, 13–15].

In this regime, the kinetic energy is negligible and Coulomb interactions dominate, giving rise to a rich correlated phase diagram hosting superconductivity, correlated insulators, and topological insulating phases [19, 39–41] as seen in Fig. 2.1.

2.2 Atomic Quasiperiodicity in Moiré systems

Since the first theoretical models for tBLG, most research has focused on commensurate structures, i.e. crystalline structures that have a well-defined unit cell (UC). However, for generic twist angles, tBLG lacks a well-defined UC [11, 14, 15] and instead exhibits atomic-scale quasiperiodicity. At the moiré scale, the tBLG "appears" to have a periodicity associated with the moiré length, which breaks down at the atomic level where its quasiperiodic nature emerges.

Despite the intrinsic quasiperiodicity of tBLG, standard approaches for studying its electronic

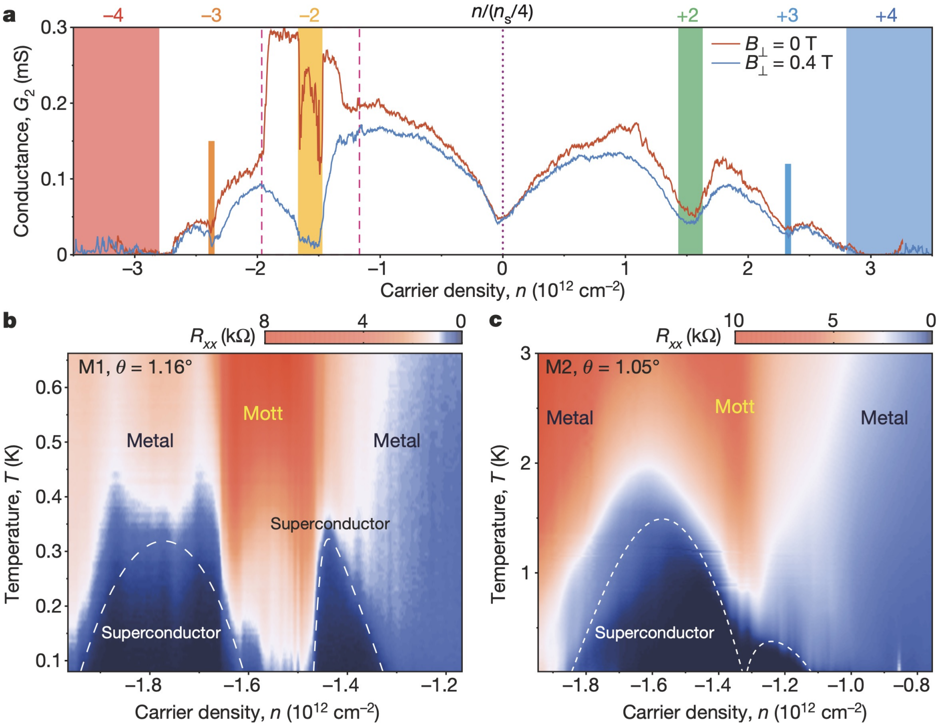

Figure 2.1: Gate-tunable superconductivity in magic-angle TBG. **(a)** Two-probe conductance $G_2 = I/V_{bias}$ of device $M1$ (ϑ=1.16°) measured in zero magnetic field (red) and at a perpendicular field of $B_\perp = 0.4T$ (blue). **(b)** Four-probe resistance R_{xx}, measured at densities corresponding tothe region bounded by pink dashed lines in a, versus temperature. **(c)** As in b, but for device $M2$, showing two asymmetric and overlapping domes. The highest critical temperature in this device is $T_c = 1.7K$. This image and text was adapted from Ref. [19].

properties have been density functional theory (DFT) and reciprocal-space continuum models – both of which use reciprocal space to perform calculations efficiently. While DFT is a powerful *ab initio* tool, applying it to commensurate structures with unit cells containing thousands of atoms is computationally overwhelming. To circumvent this, most studies have adopted low-energy continuum models. The quasiperiodic nature of tBLG structures was recognized in 2007 [11] and again in 2011 [15]. Still, the community argued that continuum models should be equally valid for any twist angle, independently of periodicity or lack thereof. As a result, the community neglected the idea of quasiperiodic moirés, focusing on commensurate configurations or assuming that continuum models are enough to describe quasiperiodic systems, as they allow closed-form analytical expressions for all types of calculations.

The community has relied on two arguments that justify neglecting quasiperiodicity in these systems. First, the flatband energy scale is set by the moiré length, hinting that the relevant physics emerges at the moiré scale, where apparent periodicity holds. Second, lattice relaxation can drive the system to commensurate configurations, effectively restoring periodicity and validating the use of continuum models. The prevailing view has been that quasiperiodicity has little impact on low-energy electronic properties. This can be a biased point of view since, until recently, no systematic theoretical studies compared reciprocal space predictions with large-scale real-space tight-binding simulations capable of capturing the effects of atomic-scale quasiperiodicity.

In 2022, Miguel Gonçalves employed a real-space tight-binding approach to tBLG, demonstrating the existence of sub-ballistic transport in quasiperiodic tBLG [42], phenomena unable to be described by continuum models. In the narrow band regime, quasiperiodic tBLG exhibits sub-ballistic states – delocalized states in both real and reciprocal space – which have suppressed transport relative to ballistic behavior. These states are accompanied by non-Poissonian energy level statistics, in sharp contrast to the ballistic transport observed at commensurate twist angles. These results are robust and distinguishable from conventional sources of disorder, highlighting a fundamental localization property of quasiperiodic moiré systems.

Quasiperiodicity-induced localization phenomena have also been reported for a twist angle of $\theta = 30^{\text{o}}$, where tBLG forms a quasicrystalline lattice with unique electronic properties. At this angle, the system hosts critical eigenstates that inherit the underlying 12-fold symmetry of the moiré superlattice [22, 43–45]. The emergence of critical states in quasiperiodic moiré systems extends beyond tBLG into a class of materials known as "Magic-angle semimetals" [46].

Quasiperiodic tBLG exhibits electronic properties that cannot be captured by continuum models, nor are present on commensurate structures. Yet, continuum models have described key experimental observations of tBLG at small twist angles, seemingly contradicting the idea that an accurate description must account for the underlying atomic-scale quasiperiodicity [13, 19, 47–49]. Despite the apparent paradox, quasiperiodicity plays an essential role in twisted multilayer materials such as twisted trilayer graphene (tTLG) [26], tBLG on hexagonal Boron Nitride[1] (tBLG/hBN) [50].

Twisted trilayer graphene is formed by stacking a third graphene layer on top of tBLG, thus introducing a new degree of freedom through a second twist angle. With three twisted layers, the two moiré patterns compete, resulting in a moiré-of-moiré (MoM) length scale, which can be significantly larger than the original moiré length of tBLG [51–54]. These two moiré patterns are generally incommensurate, leading to complex quasiperiodic structures that host electronic states beyond the scope of conventional Bloch theory, as continuum models lack a well-defined first Brillouin zone (FBZ) [52]. Moreover, tTLG hosts an infinite set of magic-angle pairs, where the low energy VHS merge into flatbands at the charge neutrality point [55, 56], providing a perfect platform to explore quasiperiodic correlated phases[52, 57]. In this manner, experimental studies observed correlated insulators and superconducting phases in quasiperiodic tTLG [23, 26].

Overall, theoretical models often disregard the role of quasiperiodicity in moiré and MoM materials, with reciprocal space continuum models remaining the primary tool for describing multilayer Van der Waals materials. This research proposal seeks to fill this gap by employing real-space techniques capable of capturing the underlying quasiperiodicity of these structures.

2.3 Lattice Relaxation in Moiré materials

In moiré materials, a crucial effect that is often neglected is lattice relaxation. When crystals are subjected to a periodic potential, such as that generated by a second layer, their lattice structure might adjust to accommodate the potential. In Ref. [50], the authors presented an example of this phenomenon and observed relaxation effects in graphene on hBN (G/hBN). The honeycomb lattice of hBN has a lattice parameter approximately $\delta \approx 1.8\%$ larger than that of graphene.

---

[1] hBN

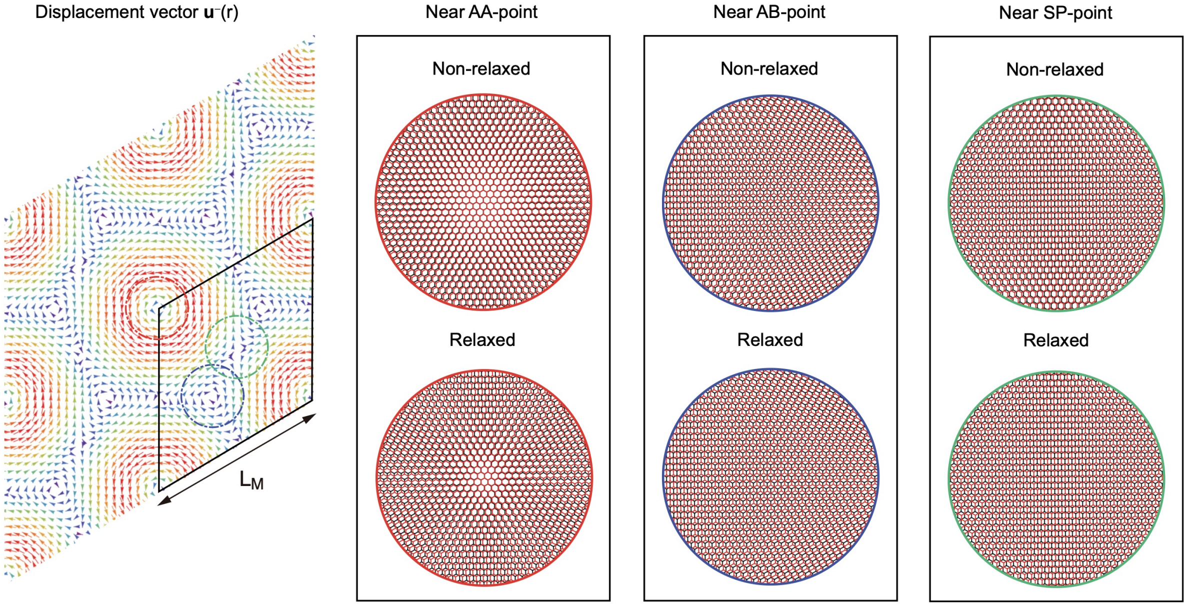

Figure 2.2: **Left side panel:** Distribution of the displacement vector $\mathbf{u}^{-}(r)$ in the tBLG of $\theta = 1.05^{\text{o}}$. **Right side panels:** Local atomic structure near AA (AB or SP) stacked point before and after the relaxation. The small dashed circles in the center panel indicate the areas where the local structure is sampled. The image and label were adapted from Ref. [58].

For small twist angles ($\theta < \delta$), graphene locally stretches to form large ($> 10nm$) commensurate stacking domains, separated by strain-concentrated domain walls. For large twist angles ($\theta > \delta$), relaxation effects become negligible, and the sample exhibits quasiperiodic behavior. In tBLG, lattice relaxation at small twist angles minimizes AA stacking regions (Fig. 2.2), increases the flatness and isolation of the lowest-energy bands, and lowers the critical angle at which the Fermi velocity vanishes [58]. A similar behavior has been reported in simulations of helical and alternating[2] tTLG [59, 60].

MoM systems exhibit intricate relaxation phenomena. Unlike tBLG, which relaxes to periodic structures near the magic angles, MoM materials exhibit a broad range of relaxed structures. Most notably, flatbands can be observed in regimes where the relaxed system retains its original quasiperiodicity [61]. In Ref. [61], the authors perform a detailed study characterizing lattice relaxation effects across a wide range of twist angle pairs. This work identifies three distinct regimes: effective periodic bilayers, periodic polycrystals, and quasicrystals (distinct from the quasicrystalline regimes discussed in [62, 63]). Most importantly, the considered twist angle pairs are compared to previous experimental results, showcasing that superconducting and correlated topological phases have been observed in quasiperiodic regimes of tTLG [26, 64].

2.4 Transport

Optical conductivity measurements trace their origins to the Drude model [65], which, in the early 20th century, accurately predicted the Drude weight of an ideal metal. Since then, these measurements have remained a key quantity for experimentalists and theorists. Researchers continue to apply established techniques to new materials while developing new ways to probe electronic properties. Moiré materials brought new challenges for transport studies. Their intricate spectral properties and high tunnability influence optical behavior and open up vast possibilities for exploring new physics.

---

[2] Helical: equal twist angles ($\theta_{12}/\theta_{23} = 1$); Alternating: symmetric twist angles ($\theta_{12}/\theta_{23} = -1$)

Since the theoretical introduction of tBLG, several studies have explored its transport properties [38, 66–69]. Overall, the optical response of tBLG at low frequencies (THz) and the Drude weight exhibit graphene-like behavior, further enhanced by the Van Hove singularities of tBLG [38]. However, these studies rely on continuum models, effectively overlooking the system's underlying quasiperiodicity. Similar approaches have been extended to other moiré materials [70], yet they encounter the same limitations, struggling to describe the sub-ballistic transport of the narrow bands.

2.5 Experimental measurements

Our current understanding of physics stems from the interplay between theoretical predictions and experimental observations. Experimentalists utilize a broad range of measurement techniques, typically sorted into two categories – local and global probes.

Global probes measure spatially averaged physical quantities on the micrometer (μm) to millimeter (mm) scale ideal for characterizing bulk properties, phase transitions, and collective phenomena. Notable examples include transport measurements [19, 21, 23, 26, 41], and capacitance/compressibility measurements [31].

In contrast, local probes offer spatial resolution from the sub-μm down to the sub-nm scale – as in STM/STS measurements – enabling spatially resolved insights into the electronic structure. Local probes are particularly useful for detecting extrinsic inhomogeneities often common in moiré systems [71]. More crucially, they reveal intrinsic inhomogeneities that arise from the properties of moiré materials [72].

The spatial resolution of local probes helps distinguish different electronic phases, which would otherwise appear identical in global probe measurements. For example, consider the following case where a transport measurement indicates an insulating phase. For the same insulating phase, STM and STS can use the local density of states (LDOS) to distinguish between charge-density wave states in $NbSe_2$ [73, 74], Mott insulating states in $TaSe_2$ [75] and Kekulé spiral state in MAtBLG [20, 39, 76].

A key quantity in probing moiré systems are transport measurements, which serve as global probes of electronic behavior and are often used to identify correlated phases. Without a solid theoretical understanding of how quasiperiodicity impacts transport – especially at finite frequencies – the interpretation of these measurements remains ambiguous.

The most common approaches are resistance and conductance measurements [19, 26]. However, accessing the optical response associated with the flatband bandwidth ($\approx 30meV$) requires probing frequencies in the far-infrared (FIR) range ($0.3-20THz$,or $1.2-83meV$, or $15-1000\mu m$). Typical sample sizes range from $2\mu m$ to $30\mu m$, depending on the fabrication methods (e.g., tear-and-stack or CVD), twist angle configuration, and measurement technique.

These frequency intervals pose a serious challenge for transport experiments: the mismatch between photon wavelength ($300\mu m$ at $1THz$, or $4meV$) and sample dimensions ($< 30\mu m$) ne-

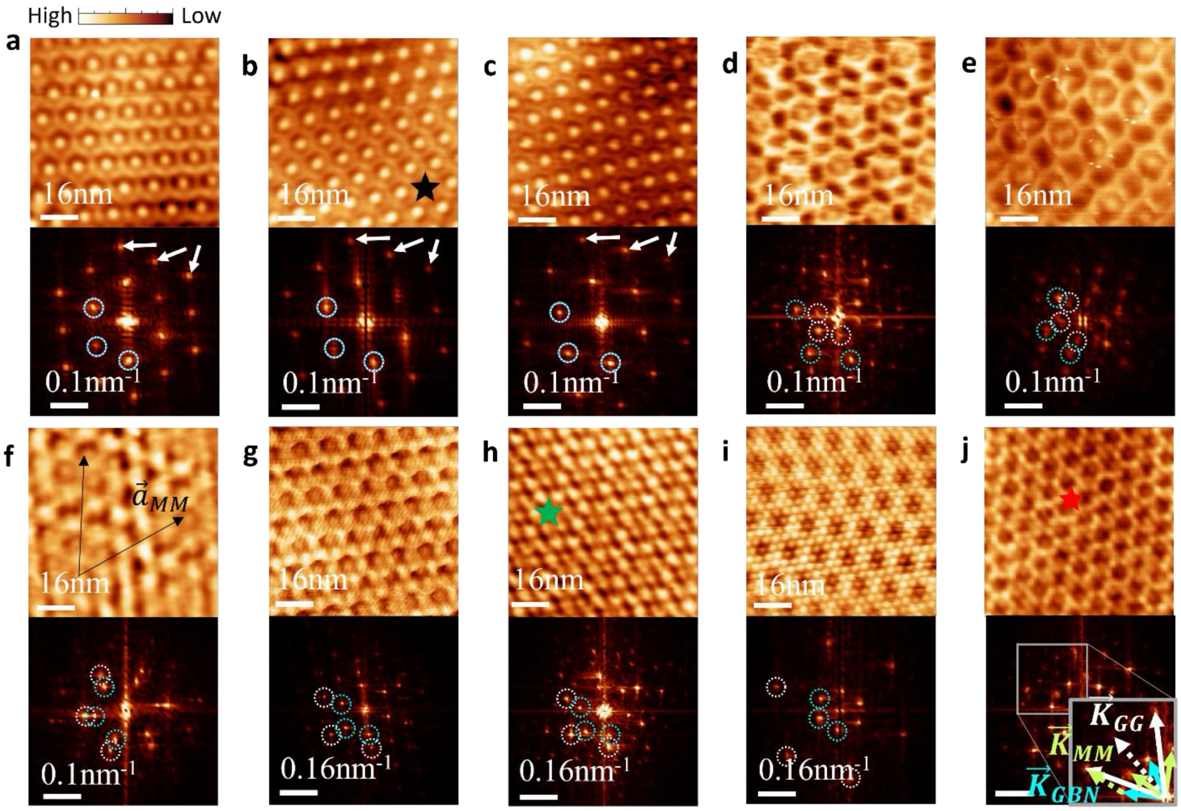

Figure 2.3: Double moiré patterns. STM topography and the corresponding FFT are shown in the top and bottom panels, respectively. **(a-c)** 1:1 commensurate moiré crystals. White arrows point to second-order Bragg peaks. **(d-i)** Moiré intercrystals (MIC). Both tBLG (GG) and graphene/hBN (GBN) periods are visible and the corresponding reciprocal lattice vectors $\vec{K}_{GG}$ and $\vec{K}_{GBN}$ are marked in the FFT with white and blue circles, respectively. **(j)** Moiré quasircrystal (MQC). Inset: Zoom-in to the grey rectangle of the FFTs. The GG, GBN, and moiré-of-moiré wavevectors, $\vec{K}_{GG}$, $\vec{K}_{GBN}$ and $\vec{K}_{MM}$, are marked with white, blue and green arrows. The image and label were adapted from Ref. [62].

cessitates near-field approaches [77] through which extracting the conductivity spectra is often difficult. Additionally, signal contamination from the THz response of the gate material further complicates the analysis. In Ref. [78], the authors introduced a new technique capable of surpassing these difficulties and performed THz conductivity measurements of a TMD monolayer (WSe_2). Another promising approach is scattering-type scanning near-field optical microscopy (s-SNOM) combined with vertical conductivity current imaging using conductive atomic force microscopy (c-AFM), which has enabled accurate terahertz conductivity measurements and gained significant attention in recent years [77, 79–81] . Overall, transport measurements capable of probing the energy range of moiré materials flatbands ($\approx 30meV$) face several constraints, with recent works opening new pathways for probing these frequencies.

Regarding local probes, recent experimental work further emphasizes the importance of accounting for quasiperiodicity in multilayered moiré materials, as this effect has profound implications for transport properties. For instance, in Ref. [62, 63, 82], the authors performed STM and STS measurements to probe the topography and LDOS in tBLG/hBN, revealing distinct structural domains: commensurate, intercrystal, and quasicrystal regimes (Fig. 2.3).

Commensurate structures in tBLG/hBN should only appear for one configuration of twist angle pairs since hBN has a small lattice parameter mismatch with graphene. However, the commensurate regimes were observed for a wide range of twist angle pairs, indicating strong relaxation effects. In contrast, the intercrystal and quasicrystal regimes break translational symmetry and are characterized by the presence or lack of Bravais lattice symmetries, respectively. In particular, the quasicrystal exhibits 12-fold rotational symmetry similar to dodecagonal tBLG ($\theta = 30^{\underline{\mathrm{o}}}$), while the intercrystal only exhibits the permissible rotational symmetries of the moiré superlattice. Moreover, the authors performed a fast Fourier transform (FFT) of the LDOS data[3], observing Bragg "like" peaks for energies near the CNP. The QPI of the commensurate crystals shows six primary Bragg peaks and twelve second-order peaks directly resulting from the perfect alignment of the tBLG and graphene/hBN moiré patterns.

The quasiperiodic crystals also display similar well-defined peaks indicative of the long-range moiré order accompanied by additional peaks since the lattice is spanned by more than two linearly independent vectors, a hallmark of quasiperiodic systems.

Global and local probes are complementary tools for characterizing moiré materials. A comprehensive understanding of their electronic phases relies on aligning theoretical predictions with experimentally accessible observables. Global probes, such as transport measurements, provide bulk property insights, while local probes, like STM and STS, offer high-resolution spatial information. In this manner, combining local and global measurements provides a comprehensive description of moiré materials.

---

[3] Known as the quasi particle interference (QPI) spectrum

Chapter 3

Research proposal

3.1 Main Goals

As discussed in chapter 2, quasiperiodicity plays a central role in shaping the electronic and spectral properties of moiré materials, both at the single-particle and many-body levels. The role of quasiperiodicity in systems like tBLG is nuanced since lattice relaxation effects generate commensurate structures. Nevertheless, studying the effects of relaxation on quasiperiodic moiré structures is relevant, particularly in the narrow-band regime where sub-ballistic states emerge. In contrast, MoM materials retain quasiperiodicity even after relaxation. These exotic structural features affect the electronic properties and produce unique signatures in experimental observables. The goal of this project is to identify quasiperiodicity-driven signatures in experimentally accessible observables, with a focus on MoM systems where these effects are especially relevant. Specifically, this proposal has four main objectives

1. Develop numerical methods capable of performing real-space tight-binding (TB) simulations of quasiperiodic systems with millions of atoms 10^6;
2. Perform detailed studies of the electronic properties of commensurate and quasiperiodic tBLG, tTLG, and tBLG/hBN, and evaluate their stability under general lattice relaxation effects;
3. Identify distinct electronic features of quasiperiodic moiré systems and link them to measurable experimental observables;
4. Bridge experimentally accessible observables with theoretical quantities – such as the inverse participation ratio and fractal dimensions – that are commonly used to characterize quasiperiodic systems but lack direct experimental counterparts.

The outcome of this PhD project will advance the current understanding of quasiperiodic moiré systems by providing theoretical predictions that guide future experimental efforts in moiré and MoM materials.

3.2 Challenges and Methodology

Challenges

Simulating quasiperiodic moiré materials presents a major challenge. Accurate modeling requires system sizes with several moiré cells – often exceeding 10^6 atoms. Even in commensurate narrow-band tBLG, the unit cell contains thousands of atoms. In such cases, translation invariance allows the application of Bloch's theorem, which significantly reduces the computational complexity. However, in quasiperiodic structures, the lack of a UC hinders the application of Bloch's theorem. As a result, real-space tight-binding simulations over millions of atoms become the only viable approach [42], posing a major computational bottleneck.

Proposed Methodology

To tackle the described challenges several approaches will be considered.

Exploitation of sparsity of tight binding Hamiltonians: Tight binding systems feature exponentially suppressed hopping amplitudes, resulting in highly sparse Hamiltonian matrices. For the required system sizes dense diagonalization needs over 16 TB of system memory and thousands of CPU hours, which is beyond the capability of high-performance computing centers. Since the focus is on the narrow bands near the Fermi level, I will use Krylov-Schur subspace methods [83], which exploit matrix sparsity to efficiently compute a fraction of the eigenvalues and eigenstates of the Hamiltonian matrix.

To push the current limit of real-space simulations – systems with10^7 atoms – I will employ kernel polynomial methods (KPM) [84] to leverage the efficiency of sparse matrix-vector products. KPM enables efficient computation of the density of states (DOS), the local DOS (LDOS), Kubo-Greenwood optical conductivity, and a fraction of the eigenstates and eigenvalues of the system.

Plane-Wave Expansion (PWE): Plane-wave expansion methods are widely employed to study moiré and multi-moiré systems [26, 52, 85]. In ballistic quasiperiodic bands, PWE converges with a finite number of plane waves and accurately describes the corresponding physics. However, in magic-angle tBLG, where sub-ballistic narrow-band states emerge, convergence requires an infinite number of plane waves. Although an analytical resummation could capture these states, closed-form expressions are generally impossible to obtain. For this reason, numerical implementations of PWE fail to describe sub-ballistic or localized wavefunctions due to basis truncation. Nonetheless, PWE remains a reliable tool for characterizing quasiperiodic Bloch bands with ballistic eigenstates.

Lattice Relaxation: Lattice relaxation plays a crucial role in moiré materials, significantly modifying their electronic properties relative to rigid lattice models [51, 58, 60–62]. An accurate description of moiré materials requires incorporating these effects. Several approaches have been developed to perform lattice relaxation calculations of moiré structures including configuration space approaches [51, 58, 60, 61] and the Frenkel-Kontorova model (FK-model) [86]. In the FK model, ions are treated as masses connected by springs. The relaxed configuration is obtained by minimizing the total elastic energy, which yields the displacement field $(\mathbf{u}^{-}(r))$.

Contingency Plan: The proposed real-space methods offer a wide range of tools to calculate the different electronic properties, offering redundancy across calculations. In case one method fails, another one can be used.

For systems with small twist angles, the moiré length increases significantly. Simulating these systems might not be possible due to the high computational cost of diagonalization methods. In such cases, I will adopt effective models with shorter moiré wavelengths by increasing the twist angle and appropriately renormalizing interlayer and intralayer hoppings [87].

3.3 Work Plan

Throughout this project, I will focus on several moiré and MoM materials, with emphasis on tBLG, tTLG, and tBLG/hBN. For each system, simulations will be carried out for both quasiperiodic and the nearest commensurate structures. The results will be systematically compared to identify signatures of quasiperiodicity.

Task 1 – Limitations of k-space description for quasi-periodic moiré systems: In this task, I will investigate the single-particle localization properties of tTLG and tBLG/hBN and assess the validity of the plane-wave expansion approach routinely employed in the literature.

I will start by analyzing the convergence of the single-particle electronic properties with the number of plane waves included in the expansion. Subsequently, I will implement a real-space tight-binding model for these materials to benchmark and validate the previous results.

The final goal is to establish the regimes where PWE fails to capture the physics of quasiperiodic systems, thereby motivating the use of real-space methods.

Task 2 – Effect of quasiperiodicity in observables of moiré systems: The goal of this task is to identify and study experimentally accessible observables that can differentiate quasiperiodic and commensurate tBLG, tTLG, and tBLG/hBN structures. In particular, I will analyze and compute these observables for experimentally relevant twist angles, focusing on:

Scanning Tunneling Spectroscopy (STS): I will compute the local density of states (LDOS) related to the STS signal and analyze the resulting data. My PhD colleagues Ricardo Oliveira and Nicolau Sobrosa are exploring a multifractal analysis of the LDOS that enables the calculation of the singularity spectrum of the wavefunction from the STS signal.

Quasi-particle interference (QPI): I will compute the FFT of the LDOS fluctuations known as the QPI and compare it to experimental data. Narrow-band states, localized in AA regions, form a hexagonal moiré superlattice. As a result, the QPI yields Bragg-like peaks that convey information regarding the properties of these eigenstates. For commensurate structures, the QPI data exhibits Bragg peaks of a hexagonal lattice with 6 -fold rotational symmetry, while quasicrystals exhibit a prohibited Bravais 12 -fold rotational symmetry [62].

Transport: I will compute the optical conductivity using the real-space Kubo-Greenwood formalism, focusing on the low-energy regime where sub-ballistic states emerge in quasiperiodic structures. This study will consider a wide range of frequencies, temperatures, and filling factors encompassing the entire narrow band range. Specifically, I will focus on the following aspects of the optical conductivity:

- Drudge Weight: I will extract the Drude weight from conductivity calculations and analyze its temperature and filling dependence. In a ballistic narrow-band, the Drude weight is suppressed due to the small Fermi velocity (or high mass). In a sub-ballistic narrow-band, the Drude weight is algebraically suppressed with system size due to the nature of the eigenstates. Additionally, I will explore methods for estimating the Drude weight from simulations of open boundary systems [88, 89], since trilayer structures are incompatible with periodic boundary arrangements.
- Conductivity Sum Rules: I will examine and verify conductivity sum rules that yield relevant quantities such as the Kohn and single-particle localization length [90, 91]. Subsequently, I will analyze the sum rules dependence on temperature, filling, and twist angle.
- Frequency dependent optical conductivity: I will study the properties of the Kubo optical conductivity, looking for unique signatures of quasiperiodicity.

Angle-resolved photoemission spectroscopy (ARPES): I will calculate the kDOS – LDOS calculated from the Fourier transformed wavefunctions. The kDOS is extracted from ARPES and nano-ARPES measurements and provides a detailed map of the band structure. This tool is particularly useful for visually distinguishing the regions of the spectrum where quasiperiodicity plays a significant role, offering valuable insight into the underlying electronic structure of the system.

Task 3: Lattice Relaxation in quasi-periodic moiré systems The goal of this task is to evaluate the effects of lattice relaxation on the electronic properties of moiré and MoM materials. I will start by considering different relaxation models, including the configuration space approach and the FK model, and compare the relaxed structures produced by each model. Subsequently, I will study the effects of lattice relaxation on the electronic properties and the considered experimental observables.

The final goal is to establish a set of real-space models capable of explaining the properties of quasiperiodic moiré and MoM systems.

Bibliography

[1] P. R. Wallace, Physical Review **71**, 622 (1947).

[2] L. D. Landau, Zh. Eksp. Teor. Fiz. **7**, 19 (1937).

[3] R. Peierls, Annales de l'institut Henri Poincaré **5**, 177 (1935).

[4] K. S. Novoselov, A. K. Geim, S. V. Morozov, D. Jiang, Y. Zhang, S. V. Dubonos, I. V. Grigorieva, and A. A. Firsov, Science **306**, 666 (2004).

[5] J. C. Meyer, A. K. Geim, M. I. Katsnelson, K. S. Novoselov, T. J. Booth, and S. Roth, Nature **446**, 60 (2007).

[6] A. Calogeracos and N. and Dombey, Contemporary Physics **40**, 313 (1999).

[7] J.-B. Zuber and C. Itzykson, *Quantum Field Theory* (Courier Corporation, 2012).

[8] P. A. Lee and T. V. Ramakrishnan, Reviews of Modern Physics **57**, 287 (1985).

[9] H. B. Heersche, P. Jarillo-Herrero, J. B. Oostinga, L. M. K. Vandersypen, and A. F. Morpurgo, Nature **446**, 56 (2007).

[10] A. H. Castro Neto, F. Guinea, N. M. R. Peres, K. S. Novoselov, and A. K. Geim, Reviews of Modern Physics **81**, 109 (2009).

[11] J. M. B. Lopes dos Santos, N. M. R. Peres, and A. H. Castro Neto, Physical Review Letters **99**, 256802 (2007).

[12] G. Binnig, H. Rohrer, Ch. Gerber, and E. Weibel, Physical Review Letters **50**, 120 (1983).

[13] G. Li, A. Luican, J. M. B. Lopes dos Santos, A. H. Castro Neto, A. Reina, J. Kong, and E. Y. Andrei, Nature Physics **6**, 109 (2010).

[14] J. M. B. Lopes dos Santos, N. M. R. Peres, and A. H. Castro Neto, Physical Review B **86**, 155449 (2012).

[15] R. Bistritzer and A. H. MacDonald, Proceedings of the National Academy of Sciences **108**, 12233 (2011).

[16] L. A. Gonzalez-Arraga, J. L. Lado, F. Guinea, and P. San-Jose, Physical Review Letters **119**, 107201 (2017).

[17] J. González, Physical Review B **88**, 125434 (2013).

[18] K. Kim, M. Yankowitz, B. Fallahazad, S. Kang, H. C. P. Movva, S. Huang, S. Larentis, C. M. Corbet, T. Taniguchi, K. Watanabe, S. K. Banerjee, B. J. LeRoy, and E. Tutuc, Nano Letters **16**, 1989 (2016).

[19] Y. Cao, V. Fatemi, S. Fang, K. Watanabe, T. Taniguchi, E. Kaxiras, and P. Jarillo-Herrero, Nature **556**, 43 (2018).

[20] J. P. Hong, T. Soejima, and M. P. Zaletel, Physical Review Letters **129**, 147001 (2022).

[21] J. Finney, A. L. Sharpe, E. J. Fox, C. L. Hsueh, D. E. Parker, M. Yankowitz, S. Chen, K. Watanabe, T. Taniguchi, C. R. Dean, A. Vishwanath, M. A. Kastner, and D. Goldhaber-Gordon, Proceedings of the National Academy of Sciences **119**, e2118482119 (2022).

[22] S. Pezzini, V. Mišeikis, G. Piccinini, S. Forti, S. Pace, R. Engelke, F. Rossella, K. Watanabe, T. Taniguchi, P. Kim, and C. Coletti, Nano Letters **20**, 3313 (2020).

[23] J. M. Park, Y. Cao, K. Watanabe, T. Taniguchi, and P. Jarillo-Herrero, Nature **590**, 249 (2021).

[24] A. T. Pierce, Y. Xie, J. M. Park, Z. Cai, K. Watanabe, T. Taniguchi, P. Jarillo-Herrero, and A. Yacoby, Tunable interplay between light and heavy electrons in twisted trilayer graphene (2024), arXiv:2401.12284 [cond-mat] .

[25] S. Turkel, J. Swann, Z. Zhu, M. Christos, K. Watanabe, T. Taniguchi, S. Sachdev, M. S. Scheurer, E. Kaxiras, C. R. Dean, and A. N. Pasupathy, Science **376**, 193 (2022).

[26] A. Uri, S. C. de la Barrera, M. T. Randeria, D. Rodan-Legrain, T. Devakul, P. J. D. Crowley, N. Paul, K. Watanabe, T. Taniguchi, R. Lifshitz, L. Fu, R. C. Ashoori, and P. Jarillo-Herrero, Nature **620**, 762 (2023).

[27] J. C. Hoke, Y. Li, Y. Hu, J. May-Mann, K. Watanabe, T. Taniguchi, T. Devakul, and B. E. Feldman, Imaging supermoire relaxation and conductive domain walls in helical trilayer graphene (2024), arXiv:2410.16269 .

[28] L. Wang, A. H. Qureshi, Y. Sun, X. Xu, X. Yao, X. Zhao, A.-L. He, Y. Zhou, and X. Zhang, Second-order topological insulator in Bilayer borophene (2024), arXiv:2407.10432 [cond-mat] .

[29] L. Wang, E.-M. Shih, A. Ghiotto, L. Xian, D. A. Rhodes, C. Tan, M. Claassen, D. M. Kennes, Y. Bai, B. Kim, K. Watanabe, T. Taniguchi, X. Zhu, J. Hone, A. Rubio, A. N. Pasupathy, and C. R. Dean, Nature Materials **19**, 861 (2020).

[30] J. Cai, E. Anderson, C. Wang, X. Zhang, X. Liu, W. Holtzmann, Y. Zhang, F. Fan, T. Taniguchi, K. Watanabe, Y. Ran, T. Cao, L. Fu, D. Xiao, W. Yao, and X. Xu, Nature **622**, 63 (2023).

[31] Y. Zeng, Z. Xia, K. Kang, J. Zhu, P. Knüppel, C. Vaswani, K. Watanabe, T. Taniguchi, K. F. Mak, and J. Shan, Nature **622**, 69 (2023).

[32] A. Ghiotto, E.-M. Shih, G. S. S. G. Pereira, D. A. Rhodes, B. Kim, J. Zang, A. J. Millis, K. Watanabe, T. Taniguchi, J. C. Hone, L. Wang, C. R. Dean, and A. N. Pasupathy, Nature **597**, 345 (2021).

[33] Y. Xu, K. Kang, K. Watanabe, T. Taniguchi, K. F. Mak, and J. Shan, Nature Nanotechnology **17**, 934 (2022).

[34] H. Li, Z. Xiang, M. H. Naik, W. Kim, Z. Li, R. Sailus, R. Banerjee, T. Taniguchi, K. Watanabe, S. Tongay, A. Zettl, F. H. da Jornada, S. G. Louie, M. F. Crommie, and F. Wang, Nature Materials **23**, 633 (2024).

[35] P. Wang, G. Yu, Y. H. Kwan, Y. Jia, S. Lei, S. Klemenz, F. A. Cevallos, R. Singha, T. Devakul, K. Watanabe, T. Taniguchi, S. L. Sondhi, R. J. Cava, L. M. Schoop, S. A. Parameswaran, and S. Wu, Nature **605**, 57 (2022).

[36] G. Yu, P. Wang, A. J. Uzan-Narovlansky, Y. Jia, M. Onyszczak, R. Singha, X. Gui, T. Song, Y. Tang, K. Watanabe, T. Taniguchi, R. J. Cava, L. M. Schoop, and S. Wu, Nature Communications **14**, 7025 (2023).

[37] E. Anderson, F.-R. Fan, J. Cai, W. Holtzmann, T. Taniguchi, K. Watanabe, D. Xiao, W. Yao, and X. Xu, Science **381**, 325 (2023).

[38] T. Stauber, P. San-Jose, and L. Brey, New Journal of Physics **15**, 113050 (2013), arXiv:1307.4606 [cond-mat] .

[39] D. Călugăru, N. Regnault, M. Oh, K. P. Nuckolls, D. Wong, R. L. Lee, A. Yazdani, O. Vafek, and B. A. Bernevig, Physical Review Letters **129**, 117602 (2022).

[40] X. Zhang, J. H. Wilson, and M. S. Foster, Physical Review B **111**, 024207 (2025), arXiv:2406.06676 [cond-mat] .

[41] M. Yankowitz, S. Chen, H. Polshyn, Y. Zhang, K. Watanabe, T. Taniguchi, D. Graf, A. F. Young, and C. R. Dean, Science **363**, 1059 (2019).

[42] M. Gonçalves, H. Z. Olyaei, B. Amorim, R. Mondaini, P. Ribeiro, and E. V. Castro, 2D Materials **9**, 011001 (2021).

[43] W. Yao, E. Wang, C. Bao, Y. Zhang, K. Zhang, K. Bao, C. K. Chan, C. Chen, J. Avila, M. C. Asensio, J. Zhu, and S. Zhou, Proceedings of the National Academy of Sciences **115**, 6928 (2018).

[44] P. Moon, M. Koshino, and Y.-W. Son, Physical Review B **99**, 165430 (2019).

[45] G. Yu, Z. Wu, Z. Zhan, M. I. Katsnelson, and S. Yuan, npj Computational Materials **5**, 1 (2019).

[46] Y. Fu, E. J. König, J. H. Wilson, Y.-Z. Chou, and J. H. Pixley, npj Quantum Materials **5**, 1 (2020).

[47] G. Sharma, I. Yudhistira, N. Chakraborty, D. Y. H. Ho, M. M. A. Ezzi, M. S. Fuhrer, G. Vignale, and S. Adam, Nature Communications **12**, 5737 (2021).

[48] A. Ghosh, S. Chakraborty, R. Dutta, A. Agarwala, K. Watanabe, T. Taniguchi, S. Banerjee, N. Trivedi, S. Mukerjee, and A. Das, Nature Physics , 1 (2025).

[49] P. Lucignano, D. Alfè, V. Cataudella, D. Ninno, and G. Cantele, Physical Review B **99**, 195419 (2019).

[50] C. R. Woods, L. Britnell, A. Eckmann, R. S. Ma, J. C. Lu, H. M. Guo, X. Lin, G. L. Yu, Y. Cao, R. V. Gorbachev, A. V. Kretinin, J. Park, L. A. Ponomarenko, M. I. Katsnelson, Y. N. Gornostyrev, K. Watanabe, T. Taniguchi, C. Casiraghi, H.-J. Gao, A. K. Geim, and K. S. Novoselov, Nature Physics **10**, 451 (2014).

[51] Z. Zhu, P. Cazeaux, M. Luskin, and E. Kaxiras, Physical Review B **101**, 224107 (2020).

[52] Z. Zhu, S. Carr, D. Massatt, M. Luskin, and E. Kaxiras, Physical Review Letters **125**, 116404 (2020).

[53] M. Anđelković, S. P. Milovanović, L. Covaci, and F. M. Peeters, Nano Letters **20**, 979 (2020).

[54] N. Leconte and J. Jung, 2D Materials **7**, 031005 (2020).

[55] C. Mora, N. Regnault, and B. A. Bernevig, Physical Review Letters **123**, 026402 (2019).

[56] C.-Y. Hao, Z. Zhan, P. A. Pantaleón, J.-Q. He, Y.-X. Zhao, K. Watanabe, T. Taniguchi, F. Guinea, and L. He, Nature Communications **15**, 8437 (2024).

[57] V. T. Phong, P. A. Pantaleón, T. Cea, and F. Guinea, Physical Review B **104**, L121116 (2021).

[58] N. N. T. Nam and M. Koshino, Physical Review B **96**, 075311 (2017).

[59] J. Jang, Journal of the Korean Physical Society **85**, 727 (2024).

[60] N. Nakatsuji, T. Kawakami, and M. Koshino, Physical Review X **13**, 041007 (2023).

[61] C. Yang, J. May-Mann, Z. Zhu, and T. Devakul, Physical Review B **110**, 115434 (2024).

[62] X. Lai, G. Li, A. M. Coe, J. H. Pixley, K. Watanabe, T. Taniguchi, and E. Y. Andrei, Moiré Periodic and Quasiperiodic Crystals in Heterostructures of Twisted Bilayer Graphene and Hexagonal Boron Nitride (2024), arXiv:2412.09654 [cond-mat] .

[63] X. Lai, D. Guerci, G. Li, K. Watanabe, T. Taniguchi, J. Wilson, J. H. Pixley, and E. Y. Andrei, Imaging Self-aligned Moir\'e Crystals and Quasicrystals in Magic-angle Bilayer Graphene on hBN Heterostructures (2023), arXiv:2311.07819 [cond-mat] .

[64] L.-Q. Xia, S. C. de la Barrera, A. Uri, A. Sharpe, Y. H. Kwan, Z. Zhu, K. Watanabe, T. Taniguchi, D. Goldhaber-Gordon, L. Fu, T. Devakul, and P. Jarillo-Herrero, Nature Physics **21**, 239 (2025).

[65] P. Drude, Annalen der Physik **306**, 566 (1900).

[66] L. Wen, Z. Li, and Y. He, Chinese Physics B **30**, 017303 (2021).

[67] T. Stauber, T. Low, and G. Gómez-Santos, Physical Review Letters **120**, 046801 (2018).

[68] C. J. Tabert and E. J. Nicol, Physical Review B **87**, 121402 (2013).

[69] T. Stauber, T. Low, and G. Gómez-Santos, Physical Review B **98**, 195414 (2018).

[70] D. Margetis, G. Gómez-Santos, and T. Stauber, Physical Review B **110**, 205144 (2024), arXiv:2409.04437 [cond-mat] .

[71] C. N. Lau, M. W. Bockrath, K. F. Mak, and F. Zhang, Nature **602**, 41 (2022).

[72] K. P. Nuckolls and A. Yazdani, Nature Reviews Materials **9**, 460 (2024), arXiv:2404.08044 [cond-mat] .

[73] M. M. Ugeda, A. J. Bradley, Y. Zhang, S. Onishi, Y. Chen, W. Ruan, C. Ojeda-Aristizabal, H. Ryu, M. T. Edmonds, H.-Z. Tsai, A. Riss, S.-K. Mo, D. Lee, A. Zettl, Z. Hussain, Z.-X. Shen, and M. F. Crommie, Nature Physics **12**, 92 (2016).

[74] X. Xi, L. Zhao, Z. Wang, H. Berger, L. Forró, J. Shan, and K. F. Mak, Nature Nanotechnology **10**, 765 (2015).

[75] Y. Chen, W. Ruan, M. Wu, S. Tang, H. Ryu, H.-Z. Tsai, R. L. Lee, S. Kahn, F. Liou, C. Jia, O. R. Albertini, H. Xiong, T. Jia, Z. Liu, J. A. Sobota, A. Y. Liu, J. E. Moore, Z.-X. Shen, S. G. Louie, S.-K. Mo, and M. F. Crommie, Nature Physics **16**, 218 (2020).

[76] K. P. Nuckolls, R. L. Lee, M. Oh, D. Wong, T. Soejima, J. P. Hong, D. Călugăru, J. Herzog-Arbeitman, B. A. Bernevig, K. Watanabe, T. Taniguchi, N. Regnault, M. P. Zaletel, and A. Yazdani, Nature **620**, 525 (2023).

[77] X. Guo, K. Bertling, B. C. Donose, M. Brünig, A. Cernescu, A. A. Govyadinov, and A. D. Rakić, Applied Physics Reviews **11**, 021306 (2024).

[78] S.-D. Chen, Q. Feng, W. Zhao, R. Qi, Z. Zhang, D. Abeysinghe, C. Uzundal, J. Xie, T. Taniguchi, K. Watanabe, and F. Wang, Direct measurement of terahertz conductivity in a gated monolayer semiconductor, https://arxiv.org/abs/2409.17633v1 (2024).

[79] S. Cui, C. Jiang, Z. Zhan, T. Wilson, N. Zhang, X. Xie, S. Yuan, H. Wang, C. Lewandowski, and G. Ni, Nano Letters **24**, 11490 (2024).

[80] J. Zhang, X. Chen, S. Mills, T. Ciavatti, Z. Yao, R. Mescall, H. Hu, V. Semenenko, Z. Fei, H. Li, V. Perebeinos, H. Tao, Q. Dai, X. Du, and M. Liu, ACS Photonics **5**, 2645 (2018).

[81] R. Jing, Y. Shao, Z. Fei, C. F. B. Lo, R. A. Vitalone, F. L. Ruta, J. Staunton, W. J.-C. Zheng, A. S. Mcleod, Z. Sun, B.-y. Jiang, X. Chen, M. M. Fogler, A. J. Millis, M. Liu, D. H. Cobden, X. Xu, and D. N. Basov, Nature Communications **12**, 5594 (2021).

[82] S.-y. Li, Z. Xu, Y. Wang, Y. Han, K. Watanabe, T. Taniguchi, A. Song, T.-B. Ma, H.-J. Gao, Y. Jiang, and J. Mao, Physical Review Letters **133**, 196401 (2024).

[83] G. W. Stewart, SIAM Journal on Matrix Analysis and Applications **23**, 601 (2002).

[84] A. Weiße, G. Wellein, A. Alvermann, and H. Fehske, Reviews of Modern Physics **78**, 275 (2006).

[85] B. Amorim and E. V. Castro, Electronic spectral properties of incommensurate twisted trilayer graphene (2018), arXiv:1807.11909 [cond-mat] .

[86] O. M. Braun and Y. S. Kivshar, *The Frenkel-Kontorova Model: Concepts, Methods, and Applications* (Springer Science & Business Media, 2013).

[87] J. Vahedi, R. Peters, A. Missaoui, A. Honecker, and G. Trambly De Laissardière, SciPost Physics **11**, 083 (2021).

[88] R. Resta, Journal of Physics: Condensed Matter **30**, 414001 (2018).

[89] G. Bellomia and R. Resta, Physical Review B **102**, 205123 (2020).

[90] D. Thouless, Physics Reports **13**, 93 (1974).

[91] I. Souza, T. Wilkens, and R. M. Martin, Physical Review B **62**, 1666 (2000).